

Inventory of high-quality flat-band van der Waals materials

Jingyi Duan^{1,2,5}, Da-Shuai Ma^{3,1,2*}, Run-Wu Zhang^{1,2*}, Zeying Zhang⁴, Chaoxi Cui^{1,2}, Wei Jiang^{1,2}, Zhi-Ming Yu^{1,2} and Yugui Yao^{1,2*}

¹Centre for Quantum Physics, Key Laboratory of Advanced Optoelectronic Quantum Architecture and Measurement (MOE), School of Physics, Beijing Institute of Technology, Beijing, 100081, China.

²Beijing Key Lab of Nanophotonics and Ultrafine Optoelectronic Systems, School of Physics, Beijing Institute of Technology, Beijing, 100081, China.

³Institute for Structure and Function & Department of Physics, Chongqing University, Chongqing, 400044, China.

⁴College of Mathematics and Physics, Beijing University of Chemical Technology, Beijing, 100029, China.

⁵College of Physics and Optoelectronic Engineering, Shenzhen University, Shenzhen, 518060, China.

*Corresponding author(s). E-mail(s): mads@cqu.edu.cn;
zhangrunwu@163.com; ygyao@bit.edu.cn;

Contributing authors: duanjy0518@gmail.com;
zzy@mail.buct.edu.cn; cuichaoxi@bit.edu.cn; jiangw@bit.edu.cn;
zhiming_yu@bit.edu.cn;

Abstract

More is left to do in the field of flat bands besides proposing theoretical models. One unexplored area is the flat bands featured in the van der Waals (vdW) materials. Exploring more flat-band material candidates and moving the promising materials toward applications have been well recognized as the cornerstones for the next-generation high-efficiency devices. Here, we utilize a powerful high-throughput tool to

screen desired vdW materials based on the Inorganic Crystal Structure Database. Through layers of filtration, we obtained 861 potential monolayers from 4997 vdW materials. Significantly, it is the first example to introduce flat-band electronic properties in the vdW materials and propose three families of representative flat-band materials by mapping two-dimensional (2D) flat-band lattice models. Unlike existing screening schemes, a simple, universal rule, *i.e.*, 2D flat-band score criterion, is first proposed to efficiently identify 229 high-quality flat-band candidates, and guidance is provided to diagnose the quality of 2D flat bands. All these efforts to screen experimental available flat-band candidates will certainly motivate continuing exploration towards the realization of this class of special materials and their applications in material science.

Keywords: flat band, high-throughput, van der Waals materials

1 Introduction

Flat bands, characterized by the high density of states and quenched electronic kinetic energy, are considered as desired paradigm to explore fascinating physical phenomena such as superconductivity[1–9], charge-density-wave state[10–13], and nontrivial band topology[14–27]. The recently discovered three-dimensional (3D) compounds[28–31] with kagome lattice composed of transition-metal ions surprisingly show the coexistence of all of the intriguing phenomena, which has attracted broad interest in condensed-matter physics and material science. As these materials share kagome geometries[25, 26, 32, 33], it is naturally expected to host those well-known features of such a unique lattice model, such as flat bands and Dirac fermions. However, due to the lack of an ideal candidate that has suitable electron filling and clear kagome bands, and the complicated interactions among electrons from various sublattices, these remarkable characteristics of flat-band effects or Dirac fermions are yet been observed in the 3D kagome compounds that have a perfect geometric kagome lattice. Therefore, it remains essential to search for high-quality materials with various flat-band lattice models to pave the way for exploring exotic correlation effect due to flat band through materials characterizations.

Motivated by the unique advantages of two-dimensional (2D) materials[34–41], more recent studies of flat-band effects has been focusing on 2D systems, especially van der Waals (vdW) materials, rather than its 3D counterparts[42–46]. Moreover, the desire to miniaturize future quantum devices has stimulated great research interest in vdW materials. Known vdW materials like graphene[47] are characterized by weak interlayer interactions through vdW forces, implying that such materials could be easily exfoliated from parent 3D crystals. It presents excellent opportunities to further explore unexplored areas of physical properties[48–51] that are constrained in 3D crystals and only possible for 2D layered systems. As a prominent example, the recently reported

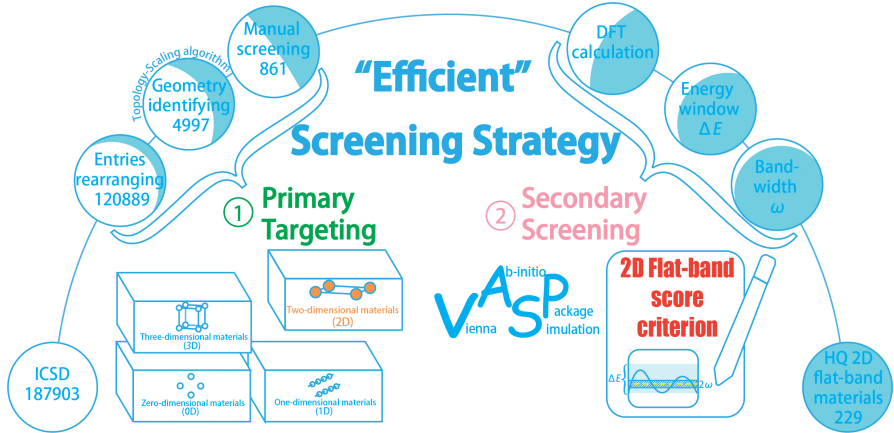


Fig. 1 The schematic flowchart of the inventory of van der Waals flat-band materials. This workflow can identify the features of flat bands and illustrate the details of constructing a high-quality (HQ) *Flat-band Materials Package* by two tiers: *primary targeting* and *secondary screening*.

twisted bilayer graphene[52–73] shows topologically nontrivial flat bands at the magic twisting angle, yielding the hallmarks of electron correlations, magnetism as well as unconventional superconductivity, which has spurred rapid development in twistrionics. Compared to 3D crystals, the 2D vdW candidates, with lower dimensional, could not only easily map out obvious flat-band lattice models but also provide more straightforward visual evidence to capture their prime features. Since vdW materials are potentially applicable for the study of flat-band effects, it is urgent to find desired realistic vdW crystals with high-quality flat band through a simple and effective approach, which could help researchers further comprehend the inherent nature of strong electron interactions.

Here, we skillfully performed high-throughput calculations to screen vdW materials with high-quality flat bands from the Inorganic Crystal Structure Database (ICSD)[74]. Starting from the 861 materials that can be easily exfoliated through the layers of filtration, we identify a subset of 229 high-quality flat-band cases according to a simple-to-use flat-band score criterion. In particular, the selected candidates display abundant structural prototypes, simple and feasible material components, covering manifold features such as magnetism, topology and superconductivity induced by the inherently strong electron interactions. Furthermore, several intriguing flat-band lattice models are presented based on selected flat-band vdW materials, including breathing kagome lattice, honeycomb lattice, and twisted-kagome lattice. Overall, the 2D high-quality flat-band candidates chosen by our research can shed new light to the intrinsic 2D flat-band physics.

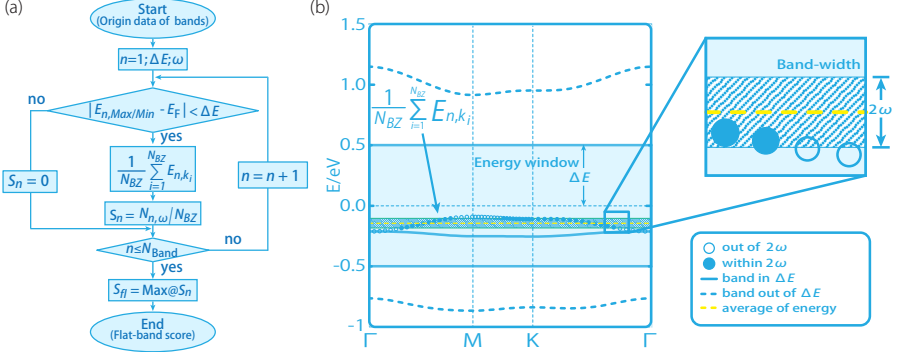


Fig. 2 (a) Workflow to construct the 2D flat-band score criterion; the core part is to determine the energy window ΔE and the band-width ω . (b) Graphical representation of the algorithm for numerically defining the flatness of band structure. Here we show the evaluation process when $\Delta E = 0.5$ eV and $\omega = 0.025$ eV. The light blue area represents the area covered by the energy window ΔE , and only the band that is wholly locating in the energy windows ΔE is scored separately. The yellow dashed line represents the average value of the energy of the band plotted in blue solid dots and blue hollow dots, and the blue and white diagonal striped area represents the effective area defined by the expansion of the yellow dashed line along with the $\pm\omega$.

2 Results

The main results of the inventory are summarized as follows. We first propose an efficient two-tier screening strategy: *primary targeting* and *secondary screening*. The former screening process mainly focuses on the selection of potential 2D candidates, *i.e.*, vdW materials, from the material database to pave the way for the deeper processing of the latter. Secondary screening aims to filter high-quality flat-band materials by first-principles calculations and our newly proposed 2D flat-band score criterion. After that, we classify the selected materials based on those intriguing properties that of general interest, including geometrical characteristics, symmetry information, conductivity, and magnetism, which could provide valuable guidance for further research. Last but not least, we showcase the three best representative flat-band materials by mapping their electronic band structure and further develop flat-band effective lattice models based on structural symmetry to unravel the main physics of the flat band.

2.1 Efficient screening strategy

There are two tiers in the high-quality vdW flat-band materials screening process: *primary targeting* (first-tier raw material targeting) and *secondary screening* (second-tier fine feature screening), as sketched in Fig. 1. Primary targeting can be further divided into three parts, namely entries rearranging, geometry identifying, and manual screening, as shown in Fig. 1 (left panel). We first excluded the seldom studied entries of the ICSD: radioactive elements, noble gas elements, elements with atomic number greater than 93, and the

entries with a total number of atoms that exceed 200. The number of targets dropped sharply from 187093 to 120889. After that, we adopted geometry identifying method to obtain vdW materials from those normal candidates. To explore the relationship between material dimensionality and the size of covalently bonded clusters, we adopt a topology-scaling algorithm[75–78] which could help us uncover the 2D structures. The results yield 4997 possible layered materials to be promising monolayers through feasible exfoliation. We finally establish a portfolio containing 861 candidates by further eliminating defective entries, and each case has a corresponding ICSD number. The details of our screening criteria are shown in the section I of *Supplementary Materials* (SM).

The secondary fine feature screening, as illustrated in Fig. 1 (right panel), is performed following first-principles calculations and 2D flat-band score criterion. In order to better extract the flat-band effective lattice model, we only focus on the cases without spin-orbit coupling. During the screening, we first collate the structural parameters and the electronic properties (band structure) of 861 candidates featuring vdW characteristics, which provides necessary guidelines for the high-throughput screening of flat-band materials. One bottleneck of current flat-band fields is to efficiently evaluate the quality of flat-band materials that can be help to advance the feasible experiments. Therefore, we further introduce a simple, universal rule for evaluating band flatness, *i.e.*, 2D flat-band score criterion, to automatically evaluate the quality of flat-band materials among 861 candidates.

To characterized the band flatness, we implement a quantitative approach to automatically search for flat-band candidates. The flat-band score for the studied material (S_{fl}) is a function of energy window (ΔE), band-width (ω), and the total number of points (N_{BZ}) along the calculated high-symmetry lines in the first Brillouin Zone (BZ). The flow chart of getting the flat-band score E_{fl} is shown in Fig. 2 (a). More specifically, it is for materials with N_{fl} bands that are totally located within the energy window $|E_{n,\text{Min/Max}} - E_F| < \Delta E$. The flat-band score of each band (S_n , n is the band index) indicates, essentially, the ratio of the number of the k -points with energy $E_{n,\mathbf{k}}$ that satisfy $|E_{n,\mathbf{k}} - \frac{1}{N_{\text{BZ}}} \sum_{i=1}^{N_{\text{BZ}}} E_{n,\mathbf{k}_i}| < \omega$ to the total k -points number N_{BZ} , which ranges from 0 to 1. Lastly, the flat-band score of the material, S_{fl} , is determined as the maximum of S_n in the energy window ΔE , as sketched in Fig. 2, which has the same range from 0 to 1 as individual band score. If a score is greater than 0, there is at least one flat band segment in the studied band structure section. For the extreme scenario, a score of 1 suggests that the candidate possesses a perfectly flat band under the prescribed conditions.

2.2 Portfolio of high-quality screened materials

With the efficient screening strategy, we have identified an extensive portfolio of high-quality monolayer structures by setting the reasonable range of ΔE and ω , as summarized in Fig. 3 (a). In this study, a combination of ΔE , ω

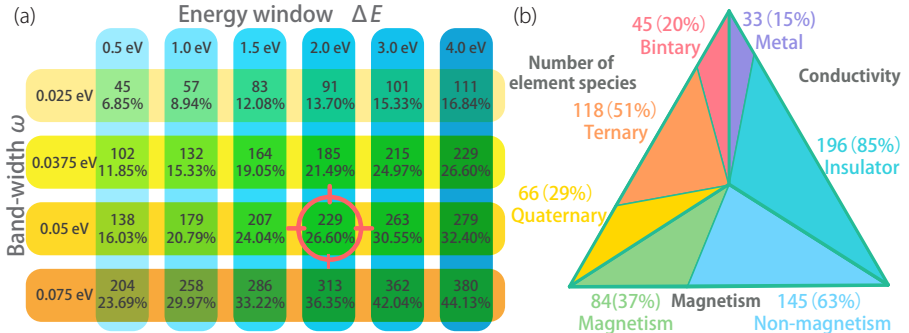


Fig. 3 (a) Distribution of high-quality flat-band materials discrete values of ω and ΔE . (b) The number of element species, conductivity and magnetism of the high-quality flat-band materials obtained by $\omega = 0.05$ eV and $\Delta E = 2$ eV are adopted.

(2 eV, 0.05 eV) is chosen as the flat-band score criterion, which searches for bands within a small energy window around the Fermi level with a reasonable small band dispersion. Without loss of generality, the results of other screening criteria are tabulated in Fig. 3 (b). Under this screening criterion, there are 229 high-quality flat-band materials that have a flat-band score greater than 0.9. To facilitate potential future researches, the 229 high-quality flat-band monolayers are further classified based on the number of elements, conductivity, and magnetism, as summarized in Fig. 3 (b). To improve the experimental feasibility, many structures are listed as candidates, including 45 binary, 118 ternary, and 66 quaternary compounds. By exploring the band structures of 229 screened materials, there are 145 (84) nonmagnetic (magnetic) materials and 196 (33) insulators (metals). The band structures of all high-quality flat-band materials are displayed in SM. Many flat bands can be easily explained theoretically via mapping flat-band lattices. This portfolio of high-quality flat-band materials offers a unique, easy-to-implement, and robust platform for exploring various intriguing properties of flat-band system.

2.3 Mapping flat-band lattices

Leveraging the 2D candidates with atomic scale, one can provide more visual evidence to capture flat-band features by mapping clearer flat-band lattices compared to the 3D system. To illustrate this, we demonstrate three representative examples from our selected high-quality flat-band materials, such as breathing-kagome lattice, honeycomb lattice, and twisted-kagome lattice to further display the physical origin of the flat bands.

The newly developed S -matrix theory[79] draws out the connection between the lattices' simple geometric features, the emergence of flat bands, and the band representation of the potential flat bands. In the S -matrix theory, a lattice is formed by two sublattices labeled by L and L', respectively. There are N_L and $N_{L'}$ ($N_{L'} < N_L$) orbitals per unit cell. Suppose the band

representations BR and BR' (formed by orbitals in L and L' sublattices) satisfy that BR-BR' is inconsistent with any band representation, the flat bands must be topological. According to the S -matrix theory, breathing-kagome lattice, honeycomb lattice, and twisted-kagome lattice have precise flat bands, which are topologically nontrivial.

From the perspective of real space, there is also one figurative understanding of the origin of the flat band in lattices models. It has been proved that we can always find compact localized states in real space to describe the flat band in breathing-kagome, honeycomb, and twisted-kagome lattices (considering only the nearest neighbor couplings). In these lattices, the number of the real space eigenstates of each flat band is $N_{\text{orbital}} + 1$, which indicates that the flat band touches with the dispersive bands at one point in BZ[80]. Based on the tight-binding (TB) Hamiltonian, more detailed explanations about the three kinds of flat-band systems are illustrated in the section III of SM.

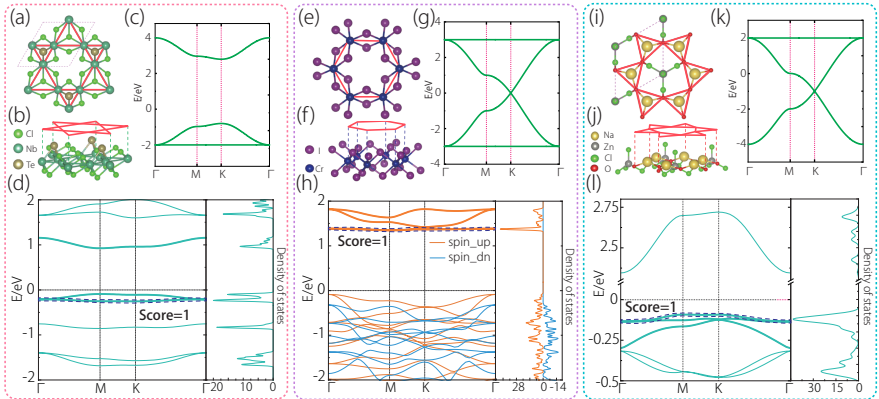


Fig. 4 The geometries of crystals and band structures in the following tangible flat-band materials. Three representative flat-band lattices involve (a, b) breathing-kagome lattice, (e, f) honeycomb lattice, and (i, j) twisted-kagome lattice. Moreover, the corresponding TB model band structure are plotted in (c, g, k), respectively. For increased visibility, prominent flat-band lattices are marked by red lines. The concrete materials include: (a, b) Nb_3TeCl_7 (icsd_079213) sharing SG 156 ($P3m1$) are identified as a breathing-kagome lattice with the Nb atoms. (d) band structure and density of states of Nb_3TeCl_7 are calculated. Similarly, (e, f) CrI_3 (icsd_251655) featuring SG 162 ($P31m$) are identified as a honeycomb lattice with the Cr atoms, and band structure and density of states are shown in (h). The orange line represents the spin-up channel, and the blue line represents the spin-down channel; (i, j) $\text{Na}_2\text{ZnO}_3\text{Cl}_4$ (icsd_024269) characterizing SG 157 ($P31m$) are identified as a twisted-kagome lattice with the O atoms, and band structure and density of states are plotted in (l).

2.3.1 Breathing-kagome lattice

Among the identified 229 high-quality flat-band materials, it is worth noting that one class is found to exhibit the characteristics of a breathing-kagome

lattice. For such type of flat-band lattice, we take Nb_3TeCl_7 as an example to explain the origin of the flat band. Since Te occupies one of the Cl hollow positions in Nb_3Cl_8 , the Nb-atoms network forms a breathing-kagome structure composed of alternating smaller downward pointing equilateral triangles and bigger upward pointing equilateral triangles, are sketched in Figs. 4 (a) and (b). In order to comprehend the key physics underlying the breathing-kagome lattice, we develop a simple three-band TB model for describing the flat-band characteristic [Fig. 4 (c)]. To better test our theoretical analysis, the band structure of Nb_3TeCl_7 is obtained from the DFT calculations [Fig. 4 (d)], which agrees well with the one of TB model. The related three bands, as highlighted in bold in Fig. 4 (d), mainly arise from the d_{z^2} orbitals of Nb, which further confirms that the flat band is indeed originated from the breathing-kagome lattice. The detailed Hamiltonians of Nb_3TeCl_7 is derived in the section III of SM.

Besides Nb_3TeCl_7 , the other M_3QX_7 family materials ($\text{M} = \text{Nb}, \text{Ta}$; $\text{Q} = \text{S}, \text{Se}, \text{Te}$; $\text{X} = \text{Cl}, \text{Br}, \text{I}$) also form the breathing-kagome lattice, which hosts a similar flat band. Furthermore, the breathing-kagome lattice contains not only non-magnetic vdW materials but also magnetic materials, such as Nb_3Cl_8 , Nb_3Br_8 and Nb_3I_8 , which could further help to reveal exotic physics of the flat band that is entangled with magnetism. More flat-band related information such as crystal structures and band structures is detailed in the section III of SM.

2.3.2 Honeycomb lattice

One of the simplest and most charming flat-band lattice is the honeycomb lattice, as diagrammed in Fig. 4 (e)-(h), which has triggered many profound physics studies. When placing the p_x and p_y (or d_{yz} and d_{xz}) atomic orbitals on the honeycomb lattice, it forms two flat bands in the band structure as shown in Fig. 4 (g). Significantly, the flat bands in many high-quality flat-band materials are derived from the p/d -band honeycomb lattice, such as the known 2D CrX_3 family with $\text{X} = \text{Cl}, \text{Br}, \text{I}$. As shown in Fig. 4(e), CrI_3 shares a honeycomb lattice where two identical sublattices are formed by the Cr atoms. Each type of Cr atom is surrounded by an octahedron formed by six iodine atoms [see Figs. 4 (e) and (f)]. With the orbital analysis, the set of bands are mainly composed by the d_{yz} and d_{xz} atomic orbitals of Cr atoms that are located on the honeycomb lattice. The flat band near 1.5 eV [(Fig. 4 (h))] is in agreement with the flat band obtained by the TB model as shown in Fig. 4 (g). Moreover, the similar flat band can be found in CrBr_3 and CrCl_3 . It is worth noting that the doping of alkali metal atoms in the vacancies of CrI_3 and CrBr_3 can adjust the relative position of the flat bands to the Fermi level[81, 82]. Thus, it is still valuable to study the properties of the flat band in CrX_3 although the flat band is intrinsically away from the Fermi level. The

crystal structures and band structures of the other CrX_3 materials are given in the section IV of SM.

2.3.3 Twisted-kagome lattice

As a deformed kagome lattice, twisted-kagome lattice is characterized by rotating adjacent site-sharing triangles in opposite directions, as is shown in Figs. 4 (i) and (j). Considering only the nearest neighbor couplings, there are a set of flat bands in the band structure of twisted-kagome lattice while putting s orbital or hybrid p orbitals on the occupied sites, as plotted in Fig. 4(k). We find that such lattice widely exists in our identified high-quality flat-band materials. Here, we describe one possible existence of flat band in a hitherto unrecognized material $\text{Na}_2\text{ZnO}_3\text{Cl}_4$. The crystal structure of $\text{Na}_2\text{ZnO}_3\text{Cl}_4$ is illustrated in Fig. 4(i) and (j), where the O atoms form a twisted-kagome lattice. The p_x and p_y orbitals of O atoms contribute to the flat band near the Fermi level [Fig. 4 (l)]. The TB model and the schematic diagram of the structure and electronic properties of this material are given in the section III of SM.

3 Discussion and Conclusion

Screened materials are real and feasible. Distinct from the existing high throughput research on flat bands[83, 84], we propose for the first time that the vdW materials are most likely to achieve flat-band characteristics. Such flat-band materials are easy to synthesize, peel, and transfer, which paves the way for future experimental studies. It is expected that the vdW materials with flat bands will provide a solid foundation for the exploration of exotic quantum phenomena (*e.g.*, such as electron correlations, magnetism, and superconductivity) and the intriguing applications of topological quantum computation in future quantum devices. Among the 229 high-quality flat-band vdW materials, many are experimentally synthesized materials with their flat band properties overlooked that awaits further experimental investigation. For example, the bulk compound Nb_3TeCl_7 has been synthesized and structurally characterized by single-crystal X-ray diffraction in 1995[85]. In such lattice, Nb atoms that contribute to the flat band are distorted from high-symmetry locations to produce trimers with shorter interatomic distances, which forms the basis of ferroelectric polarization. Lattice breathing interchanges trimer patterns that further switches the direction of ferroelectric polarization, which simultaneously remodels the flat band. Another example is CrI_3 , which has been reported as intrinsic ferromagnetism in atomically thin crystals. The family of CrX_3 ($\text{X}=\text{Cl}, \text{Br}, \text{I}$) materials exhibit plentiful intriguing properties[86–89] the giant tunneling magnetoresistance, gate tunable magneto-optical Kerr effect, and a large magnetocrystalline anisotropy. Screening results showcase that flat band vdW materials are abundant, implying the great potential for realizing flat band characteristics of different realistic applications. Future experiments could more easily access these flat bands with

a high density of states, which renders more exciting physics phenomena, such as superconductivity, charge-density-wave state, and nontrivial band topology.

Filtering strategies are unique and efficient. The recently discovered potential flat-band compounds featured by the kagome lattice composed of transition-metal ions have attracted much theoretical and experimental attention. Because of the kagome lattice of these materials, it was touted as a promising platform to detect the flat band. However, it is far more challenging to characterize the flat bands due to the lack of ideal candidates and/or vanishing flat-band feature due to many-body interaction though with a kagome lattice. It remains an open question whether one can find a convenient indicator to evaluate the flatness of the band. Once identified, such indicator can help evaluate the quality of flat bands. In this work, a simple, universal rule, *i.e.*, 2D flat-band score criterion, is proposed to identify various flat-band candidates efficiently, and guidance is provided to diagnose the quality of 2D flat bands. Significantly, our criterion can quantitatively determine the flatness of the screened vdW materials, which provide over 229 high-quality candidate materials for experimental verification.

In this work, we have performed a systematic search for flat-band vdW materials and further explored the flat-band physical mechanism by mapping the types of lattices from the vdW candidates. By implementing effective screening strategies to 861 unique monolayers, we found that 229 candidates (score criterion: $\omega = 0.05$ eV and $\Delta E = 2$ eV) host high-quality flat bands. The appearance of flat bands in materials can be, in large but non-exhaustive part, theoretically understood using the S -matrix method, as we have exemplified in three representative candidates, *i.e.*, Nb_3TeCl_7 , CrI_3 and $\text{Na}_2\text{ZnO}_3\text{Cl}_4$. Our results work as a guide for future theoretical and experimental studies on 2D flat-band materials where exotic physics phenomena such as magnetism and superconductivity can be further explored. All the results obtained in this work and detailed in the SM can be accessed on the *Flat-band Materials Package*.

References

- [1] White, S.R., Sham, L.J.: Electronic properties of flat-band semiconductor heterostructures. *Phys. Rev. Lett.* **47**(12), 879–882 (1981)
- [2] Sutherland, B.: Simple system with quasiperiodic dynamics: A spin in a magnetic field. *Phys. Rev. Lett.* **57**(6), 770–773 (1986)
- [3] Lieb, E.H.: Two theorems on the Hubbard model. *Phys. Rev. Lett.* **62**(10), 1201–1204 (1989)
- [4] Kopnin, N.B., Heikkilä, T.T., Volovik, G.E.: High-temperature surface superconductivity in topological flat-band systems. *Phys. Rev. B* **83**(22), 220503 (2011)

- [5] Tang, E., Fu, L.: Strain-induced partially flat band, helical snake states and interface superconductivity in topological crystalline insulators. *Nat. Phys.* **10**(12), 964–969 (2014)
- [6] Iglovikov, V.I., Hébert, F., Grémaud, B., Batrouni, G.G., Scalettar, R.T.: Superconducting transitions in flat-band systems. *Phys. Rev. B* **90**(9), 094506 (2014)
- [7] Volovik, G.E.: Graphite, graphene and the flat band superconductivity. *JETP Lett.* **107**(8), 516–517 (2018)
- [8] Yin, J.-X., Zhang, S.S., Chang, G., Wang, Q., Tsirkin, S.S., Guguchia, Z., Lian, B., Zhou, H., Jiang, K., Belopolski, I., Shumiya, N., Multer, D., Litskevich, M., Cochran, T.A., Lin, H., Wang, Z., Neupert, T., Jia, S., Lei, H., Hasan, M.Z.: Negative flat band magnetism in a spin-orbit-coupled correlated kagome magnet. *Nat. Phys.* **15**(5), 443–448 (2019)
- [9] Liu, X., Chiu, C.-L., Lee, J.Y., Farahi, G., Watanabe, K., Taniguchi, T., Vishwanath, A., Yazdani, A.: Spectroscopy of a tunable moiré system with a correlated and topological flat band. *Nat. Commun.* **12**(1), 2732 (2021)
- [10] Rice, T.M., Scott, G.K.: New mechanism for a charge-density-wave instability. *Phys. Rev. Lett.* **35**(2), 120–123 (1975)
- [11] Carpinelli, J.M., Weitering, H.H., Plummer, E.W., Stumpf, R.: Direct observation of a surface charge density wave. *Nature* **381**(6581), 398–400 (1996)
- [12] Calandra, M.: Phonon-assisted magnetic mott-insulating state in the charge density wave phase of single-layer 1T-NbSe₂. *Phys. Rev. Lett.* **121**(2), 026401 (2018)
- [13] Wang, W., Wang, B., Gao, Z., Tang, G., Lei, W., Zheng, X., Li, H., Ming, X., Autieri, C.: Charge density wave instability and pressure-induced superconductivity in bulk 1T-NbS₂. *Phys. Rev. B* **102**(15), 155115 (2020)
- [14] Miyahara, S., Kusuta, S., Furukawa, N.: BCS theory on a flat band lattice. *Physica C* **460-462**, 1145–1146 (2007)
- [15] Dóra, B., Kailasvuori, J., Moessner, R.: Lattice generalization of the Dirac equation to general spin and the role of the flat band. *Phys. Rev. B* **84**(19), 195422 (2011)
- [16] Wang, F., Ran, Y.: Nearly flat band with Chern number C=2 on the dice lattice. *Phys. Rev. B* **84**(24), 241103 (2011)
- [17] Bergholtz, E.J., Liu, Z.: Topological flat band models and fractional chern

- insulators. *Int. J. Mod. Phys. B* **27**(24), 1330017 (2013)
- [18] Mukherjee, S., Spracklen, A., Choudhury, D., Goldman, N., Öhberg, P., Andersson, E., Thomson, R.R.: Observation of a localized flat-band state in a photonic Lieb lattice. *Phys. Rev. Lett.* **114**(24), 245504 (2015)
- [19] Morales-Inostroza, L., Vicencio, R.A.: Simple method to construct flat-band lattices. *Phys. Rev. A* **94**(4), 043831 (2016)
- [20] Julku, A., Peotta, S., Vanhala, T.I., Kim, D.-H., Törmä, P.: Geometric origin of superfluidity in the Lieb-lattice flat band. *Phys. Rev. Lett.* **117**(4), 045303 (2016)
- [21] Mondaini, R., Batrouni, G.G., Grémaud, B.: Pairing and superconductivity in the flat band: Creutz lattice. *Phys. Rev. B* **98**(15), 155142 (2018)
- [22] Maimaiti, W., Andreanov, A., Park, H.C., Gendelman, O., Flach, S.: Compact localized states and flat-band generators in one dimension. *Phys. Rev. B* **95**(11), 115135 (2017)
- [23] Leykam, D., Andreanov, A., Flach, S.: Artificial flat band systems: from lattice models to experiments. *Adv. Phys.:X* **3**(1), 1473052 (2018)
- [24] Gardenier, T.S., van den Broeke, J.J., Moes, J.R., Swart, I., Delerue, C., Slot, M.R., Smith, C.M., Vanmaekelbergh, D.: p orbital flat band and dirac cone in the electronic honeycomb lattice. *ACS Nano* **14**(10), 13638–13644 (2020)
- [25] Chiu, C.S., Ma, D.-S., Song, Z.-D., Bernevig, B.A., Houck, A.A.: Fragile topology in line-graph lattices with two, three, or four gapped flat bands. *Phys. Rev. Research* **2**(4), 043414 (2020)
- [26] Ma, D.-S., Xu, Y., Chiu, C.S., Regnault, N., Houck, A.A., Song, Z., Bernevig, B.A.: Spin-orbit-induced topological flat bands in line and split graphs of bipartite lattices. *Phys. Rev. Lett.* **125**(26), 266403 (2020)
- [27] Čadež, T., Kim, Y., Andreanov, A., Flach, S.: Metal-insulator transition in infinitesimally weakly disordered flat bands. *Phys. Rev. B* **104**(18), 180201 (2021)
- [28] Provenzano, P.P.: Bringing order to the matrix. *Nat. Mater.* **19**(2), 130–131 (2020)
- [29] Ghimire, N.J., Dally, R.L., Poudel, L., Jones, D.C., Michel, D., Magar, N.T., Bleuel, M., McGuire, M.A., Jiang, J.S., Mitchell, J.F., Lynn, J.W., Mazin, I.I.: Competing magnetic phases and fluctuation-driven scalar spin

- chirality in the kagome metal YMn_6Sn_6 . *Sci. Adv.* **6**(51), 2680 (2020)
- [30] Lou, R., Fedorov, A., Yin, Q., Kuibarov, A., Tu, Z., Gong, C., Schvier, E.F., Büchner, B., Lei, H., Borisenko, S.: Charge-density-wave-induced peak-dip-hump structure and the multiband superconductivity in a kagome superconductor CsV_3Sb_5 . *Phys. Rev. Lett.* **128**(3), 036402 (2022)
- [31] Neupert, T., Denner, M.M., Yin, J.-X., Thomale, R., Hasan, M.Z.: Charge order and superconductivity in kagome materials. *Nat. Phys.* **18**(2), 137–143 (2022)
- [32] Mielke, A.: Ferromagnetism in the Hubbard model on line graphs and further considerations. *J. Phys. A: Math. Gen.* **24**(14), 3311–3321 (1991)
- [33] Mielke, A.: Ferromagnetic ground states for the Hubbard model on line graphs. *J. Phys. A: Math. Gen.* **24**(2), 73–77 (1991)
- [34] Chen, Y., Fan, Z., Zhang, Z., Niu, W., Li, C., Yang, N., Chen, B., Zhang, H.: Two-dimensional metal nanomaterials: Synthesis, properties, and applications. *Chem. Rev.* **118**(13), 6409–6455 (2018)
- [35] Jin, H., Guo, C., Liu, X., Liu, J., Vasileff, A., Jiao, Y., Zheng, Y., Qiao, S.-Z.: Emerging two-dimensional nanomaterials for electrocatalysis. *Chem. Rev.* **118**(13), 6337–6408 (2018)
- [36] Han, G.H., Duong, D.L., Keum, D.H., Yun, S.J., Lee, Y.H.: van der Waals metallic transition metal dichalcogenides. *Chem. Rev.* **118**(13), 6297–6336 (2018)
- [37] Zeng, M., Xiao, Y., Liu, J., Yang, K., Fu, L.: Exploring two-dimensional materials toward the next-generation circuits: From monomer design to assembly control. *Chem. Rev.* **118**(13), 6236–6296 (2018)
- [38] Zhang, H.: Introduction: 2D materials chemistry. *Chem. Rev.* **118**(13), 6089–6090 (2018)
- [39] Dong, R., Zhang, T., Feng, X.: Interface-assisted synthesis of 2d materials: Trend and challenges. *Chem. Rev.* **118**(13), 6189–6235 (2018)
- [40] Cai, Z., Liu, B., Zou, X., Cheng, H.-M.: Chemical vapor deposition growth and applications of two-dimensional materials and their heterostructures. *Chem. Rev.* **118**(13), 6091–6133 (2018)
- [41] Li, H., Li, Y., Aljarb, A., Shi, Y., Li, L.-J.: Epitaxial growth of two-dimensional layered transition-metal dichalcogenides: Growth mechanism, controllability, and scalability. *Chem. Rev.* **118**(13), 6134–6150 (2018)
- [42] Jacqmin, T., Carusotto, I., Sagnes, I., Abbarchi, M., Solnyshkov, D.D.,

- Malpuech, G., Galopin, E., Lemaître, A., Bloch, J., Amo, A.: Direct observation of dirac cones and a flat band in a honeycomb lattice for polaritons. *Phys. Rev. Lett.* **112**(11), 116402 (2014)
- [43] Wang, R.-N., Zhang, X.-R., Wang, S.-F., Fu, G.-S., Wang, J.-L.: Flat-bands in 2D boroxine-linked covalent organic frameworks. *Phys. Chem. Chem. Phys.* **18**(2), 1258–1264 (2016)
- [44] Zhang, S.M., Jin, L.: Flat band in two-dimensional non-Hermitian optical lattices. *Phys. Rev. A* **100**(4), 043808 (2019)
- [45] Crasto de Lima, F., Ferreira, G.J., Miwa, R.H.: Topological flat band, Dirac fermions and quantum spin Hall phase in 2D archimedean lattices. *Phys. Chem. Chem. Phys.* **21**(40), 22344–22350 (2019)
- [46] Maimaiti, W., Andrianov, A., Flach, S.: Flat-band generator in two dimensions. *Phys. Rev. B* **103**(16), 165116 (2021)
- [47] Geim, A.K.: Graphene: Status and prospects. *Science* **324**(5934), 1530–1534 (2009)
- [48] Guo, B., Fang, L., Zhang, B., Gong, J.R.: Graphene Doping: A Review. *Insciences J.*, 80–89 (2011)
- [49] Lazar, P., Karlický, F., Jurečka, P., Kocman, M., Otyepková, E., Šafářová, K., Otyepka, M.: Adsorption of small organic molecules on graphene. *J. Am. Chem. Soc.* **135**(16), 6372–6377 (2013)
- [50] Kong, L., Enders, A., Rahman, T.S., Dowben, P.A.: Molecular adsorption on graphene. *J. Phys.: Condens. Matter* **26**(44), 443001 (2014)
- [51] Si, C., Sun, Z., Liu, F.: Strain engineering of graphene: A review. *Nanoscale* **8**(6), 3207–3217 (2016)
- [52] Cao, Y., Fatemi, V., Fang, S., Watanabe, K., Taniguchi, T., Kaxiras, E., Jarillo-Herrero, P.: Unconventional superconductivity in magic-angle graphene superlattices. *Nature* **556**(7699), 43–50 (2018)
- [53] Xu, C., Balents, L.: Topological superconductivity in twisted multilayer graphene. *Phys. Rev. Lett.* **121**, 087001 (2018)
- [54] Zou, L., Po, H.C., Vishwanath, A., Senthil, T.: Band structure of twisted bilayer graphene: Emergent symmetries, commensurate approximants, and wannier obstructions. *Phys. Rev. B* **98**, 085435 (2018)
- [55] Fidrysiak, M., Zegrodnik, M., Spalek, J.: Unconventional topological superconductivity and phase diagram for an effective two-orbital model as applied to twisted bilayer graphene. *Phys. Rev. B* **98**, 085436 (2018)

- [56] Po, H.C., Zou, L., Vishwanath, A., Senthil, T.: Origin of Mott insulating behavior and superconductivity in twisted bilayer graphene. *Phys. Rev. X* **8**, 031089 (2018)
- [57] Isobe, H., Yuan, N.F.Q., Fu, L.: Unconventional superconductivity and density waves in twisted bilayer graphene. *Phys. Rev. X* **8**, 041041 (2018)
- [58] Wu, F., MacDonald, A.H., Martin, I.: Theory of phonon-mediated superconductivity in twisted bilayer graphene. *Phys. Rev. Lett.* **121**, 257001 (2018)
- [59] Laksono, E., Leaw, J.N., Reaves, A., Singh, M., Wang, X., Adam, S., Gu, X.: Singlet superconductivity enhanced by charge order in nested twisted bilayer graphene fermi surfaces. *Solid State Commun.* **282**, 38–44 (2018)
- [60] Liu, C.-C., Zhang, L.-D., Chen, W.-Q., Yang, F.: Chiral spin density wave and $d + id$ superconductivity in the magic-angle-twisted bilayer graphene. *Phys. Rev. Lett.* **121**, 217001 (2018)
- [61] Su, Y., Lin, S.-Z.: Pairing symmetry and spontaneous vortex-antivortex lattice in superconducting twisted-bilayer graphene: Bogoliubov-de Gennes approach. *Phys. Rev. B* **98**, 195101 (2018)
- [62] Peltonen, T.J., Ojajärvi, R., Heikkilä, T.T.: Mean-field theory for superconductivity in twisted bilayer graphene. *Phys. Rev. B* **98**, 220504 (2018)
- [63] Kennes, D.M., Lischner, J., Karrasch, C.: Strong correlations and $d + id$ superconductivity in twisted bilayer graphene. *Phys. Rev. B* **98**, 241407 (2018)
- [64] Guinea, F., Walet, N.R.: Electrostatic effects, band distortions, and superconductivity in twisted graphene bilayers. *Proc. Natl. Acad. Sci. U.S.A.* **115**(52), 13174–13179 (2018)
- [65] Roy, B., Jurić, V.: Unconventional superconductivity in nearly flat bands in twisted bilayer graphene. *Phys. Rev. B* **99**, 121407 (2019)
- [66] Lian, B., Wang, Z., Bernevig, B.A.: Twisted bilayer graphene: A phonon-driven superconductor. *Phys. Rev. Lett.* **122**, 257002 (2019)
- [67] González, J., Stauber, T.: Kohn-luttinger superconductivity in twisted bilayer graphene. *Phys. Rev. Lett.* **122**, 026801 (2019)
- [68] Seo, K., Kotov, V.N., Uchoa, B.: Ferromagnetic Mott state in twisted graphene bilayers at the magic angle. *Phys. Rev. Lett.* **122**, 246402 (2019)
- [69] Yankowitz, M., Chen, S., Polshyn, H., Zhang, Y., Watanabe, K.,

- Taniguchi, T., Graf, D., Young, A.F., Dean, C.R.: Tuning superconductivity in twisted bilayer graphene. *Science* **363**(6431), 1059–1064 (2019)
- [70] Lu, X., Stepanov, P., Yang, W., Xie, M., Aamir, M.A., Das, I., Urgell, C., Watanabe, K., Taniguchi, T., Zhang, G., *et al.*: Superconductors, orbital magnets and correlated states in magic-angle bilayer graphene. *Nature* **574**(7780), 653–657 (2019)
- [71] Sharpe, A.L., Fox, E.J., Barnard, A.W., Finney, J., Watanabe, K., Taniguchi, T., Kastner, M., Goldhaber-Gordon, D.: Emergent ferromagnetism near three-quarters filling in twisted bilayer graphene. *Science* **365**(6453), 605–608 (2019)
- [72] Huang, T., Zhang, L., Ma, T.: Antiferromagnetically ordered mott insulator and $d + id$ superconductivity in twisted bilayer graphene: A quantum monte carlo study. *Sci. Bull.* **64**(5), 310–314 (2019)
- [73] Wu, X.-C., Pawlak, K.A., Jian, C.-M., Xu, C.: Emergent superconductivity in the weak Mott insulator phase of bilayer graphene moiré superlattice. arXiv:1805.06906 (2018)
- [74] Belsky, A., Hellenbrandt, M., Karen, V.L., Luksch, P.: New developments in the inorganic crystal structure database (ICSD): Accessibility in support of materials research and design. *Acta Crystallogr., Sect. B: Struct. Sci.* **58**(3), 364–369 (2002)
- [75] Ashton, M., Paul, J., Sinnott, S.B., Hennig, R.G.: Topology-scaling identification of layered solids and stable exfoliated 2D materials. *Phys. Rev. Lett.* **118**(10), 106101 (2017)
- [76] Cheon, G., Duerloo, K.-A.N., Sendek, A.D., Porter, C., Chen, Y., Reed, E.J.: Data mining for new two- and one-dimensional weakly bonded solids and lattice-commensurate heterostructures. *Nano Lett.* **17**(3), 1915–1923 (2017)
- [77] Mounet, N., Gibertini, M., Schwaller, P., Campi, D., Merkys, A., Marrazzo, A., Sohler, T., Castelli, I.E., Cepellotti, A., Pizzi, G., Marzari, N.: Two-dimensional materials from high-throughput computational exfoliation of experimentally known compounds. *Nature* **13**(3), 246–252 (2018)
- [78] Zhu, Y., Kong, X., Rhone, T.D., Guo, H.: Systematic search for two-dimensional ferromagnetic materials. *Phys. Rev. Mater.* **2**(8), 081001 (2018)

- [79] Călugăru, D., Chew, A., Elcoro, L., Xu, Y., Regnault, N., Song, Z.-D., Bernevig, B.A.: General construction and topological classification of crystalline flat bands. *Nat. Phys.* **18**(2), 185–189
- [80] Bergman, D.L., Wu, C., Balents, L.: Band touching from real-space topology in frustrated hopping models. *Phys. Rev. B* **78**(12), 125104
- [81] Xu, Q.-F., Xie, W.-Q., Lu, Z.-W., Zhao, Y.-J.: Theoretical study of enhanced ferromagnetism and tunable magnetic anisotropy of monolayer CrI_3 by surface adsorption. *Phys. Lett. A* **384**(29), 126754 (2020)
- [82] Zhang, H., Yang, W., Ning, Y., Xu, X.: High-temperature and multichannel quantum anomalous Hall effect in pristine and alkali-metal-doped CrBr_3 monolayers. *Nanoscale* **12**(26), 13964–13972 (2020)
- [83] Regnault, N., Xu, Y., Li, M.-R., Ma, D.-S., Jovanovic, M., Yazdani, A., Parkin, S.S.P., Felser, C., Schoop, L.M., Ong, N.P., Cava, R.J., Elcoro, L., Song, Z.-D., Bernevig, B.A.: Catalogue of flat-band stoichiometric materials. *Nature* **603**(7903), 824–828 (2022)
- [84] Liu, H., Meng, S., Liu, F.: Screening two-dimensional materials with topological flat bands. *Phys. Rev. Mater.* **5**, 084203 (2021)
- [85] Miller, G.J.: Solid state chemistry of Nb_3Cl_8 : Nb_3TeCl_7 , mixed crystal formation, and intercalation. *J. Alloys Compd.*, 8 (1995)
- [86] Huang, B., Clark, G., Navarro-Moratalla, E., Klein, D.R., Cheng, R., Seyler, K.L., Zhong, D., Schmidgall, E., McGuire, M.A., Cobden, D.H., Yao, W., Xiao, D., Jarillo-Herrero, P., Xu, X.: Layer-dependent ferromagnetism in a van der Waals crystal down to the monolayer limit. *Nature* **546**(7657), 270–273 (2017)
- [87] Lin, G.T., Luo, X., Chen, F.C., Yan, J., Gao, J.J., Sun, Y., Tong, W., Tong, P., Lu, W.J., Sheng, Z.G., Song, W.H., Zhu, X.B., Sun, Y.P.: Critical behavior of two-dimensional intrinsically ferromagnetic semiconductor CrI_3 . *Appl. Phys. Lett.* **112**(7), 072405 (2018)
- [88] Shcherbakov, D., Stepanov, P., Weber, D., Wang, Y., Hu, J., Zhu, Y., Watanabe, K., Taniguchi, T., Mao, Z., Windl, W., Goldberger, J., Bockrath, M., Lau, C.N.: Raman spectroscopy, photocatalytic degradation, and stabilization of atomically thin chromium tri-iodide. *Nano Lett.* **18**(7), 4214–4219 (2018)
- [89] Thiel, L., Wang, Z., Tschudin, M.A., Rohner, D., Gutiérrez-Lezama, I., Ubrig, N., Gibertini, M., Giannini, E., Morpurgo, A.F., Maletinsky, P.: Probing magnetism in 2D materials at the nanoscale with single-spin microscopy. *Science* **364**(6444), 973–976 (2019)

- [90] Kresse, G., Furthmüller, J.: Efficiency of ab-initio total energy calculations for metals and semiconductors using a plane-wave basis set. *Comput. Mater. Sci.* **6**(1), 15–50 (1996)
- [91] Monkhorst, H.J., Pack, J.D.: Special points for Brillouin-zone integrations. *Phys. Rev. B* **13**(12), 5188–5192 (1976)
- [92] Blöchl, P.E.: Projector augmented-wave method. *Phys. Rev. B* **50**(24), 17953–17979 (1994)
- [93] Kresse, G., Furthmüller, J.: Efficient iterative schemes for *ab initio* total-energy calculations using a plane-wave basis set. *Phys. Rev. B* **54**(16), 11169–11186 (1996)
- [94] Perdew, J.P., Burke, K., Ernzerhof, M.: Generalized gradient approximation made simple. *Phys. Rev. Lett.* **77**(18), 3865–3868 (1996)
- [95] Kresse, G., Joubert, D.: From ultrasoft pseudopotentials to the projector augmented-wave method. *Phys. Rev. B* **59**(3), 1758–1775 (1999)
- [96] Calderon, C.E., Plata, J.J., Toher, C., Oses, C., Levy, O., Fornari, M., Natan, A., Mehl, M.J., Hart, G., Buongiorno Nardelli, M., Curtarolo, S.: The AFLOW standard for high-throughput materials science calculations. *Comput. Mater. Sci.* **108**, 233–238 (2015)

Methods. We performed a high-throughput computation to reveal the electronica properties of the 861 vdW materials. We use density functional theory (DFT) as implemented in the Vienna ab initio Simulation Package (VASP)[90] to calculate the band structures of the 861 2D materials. The Projector Augmented Wave (PAW) scheme with the Perdew-Burke-Ernzerhof (PBE) generalized gradient approximation (GGA) exchange-correlation function is employed [91–95]. We only focus on the DFT calculations performed without spin-orbit coupling. We adopt the GGA+ U method for the calculations, which considers the on-site Hubbard U value of d or f electron in the mean-field approximation[96].

Acknowledgments. The work is supported by the National Key R&D Program of China (Grant No. 2020YFA0308800), the National Natural Science Foundation of China (Grants Nos. 11734003, 12061131002), the Strategic Priority Research Program of Chinese Academy of Sciences (Grant No. XDB30000000) and the China Postdoctoral Science Foundation (Grant Nos.2020M680011, 2021T140057).

Competing interests. The authors declare no competing interests.

Corresponding authors. Correspondence and requests for materials should be addressed to Yugui Yao or Da-Shuai Ma or Run-Wu Zhang.